The International Journal of Advanced Manufacturing Technology, Volume 121, Issue 1-2, July 2022, pp. 1235-1251
DOI: 10.1007/s00170-022-09369-9

Optimization of Multi-Tooth Milling Tool for Interlaminar Damage Suppression in the Milling of Carbon Fiber Reinforced Polymers

Jian Liu[a], Xinkai Tang[a,b], Shipeng Li[a]*, Xuda Qin[a], Hao Li[a], Weizhou Wu[a], Yadav Srijana[a], Wentao Liu[a] Haibao Liu[c]

a Key Laboratory of Mechanism Theory and Equipment Design of Ministry of Education, Tianjin University, Tianjin, 300354, China
b China Helicopter Research and Development Institute, Jingdezhen 333000, China
c Centre for Aeronautics, School of Aerospace, Transport and Manufacturing, Cranfield University, Cranfield MK43 0AL, UK
* Corresponding author: shipengli@tju.edu.cn

Abstract

Carbon Fiber Reinforced Polymers (CFRP) is widely utilized in the aerospace field due to their significant specific strength, specific modulus and strong design ability. However, anisotropy and low interlaminar bonding strength lead to burr, tear, lamination and other damages in CFRP machining. In this paper, a 3D finite element model for the milling of CFRP was carefully developed and the cutting forces, the interlaminar stress and the interlaminar damage were properly obtained. Typically based on the developed model, the effects of geometric parameters of the multi-tooth milling tool were precisely analyzed. Next tool geometries were optimized for suppressing the interlaminar damage in the milling of CFRP. Results convincingly show that the multi-tooth milling tool with the geometry of 1.4mm length of the micro tooth, 38.2° left helix angle, 11 left-handed chip grooves, 15° right helix angle, 12 right-handed helix grooves, approximately rectangular of section shape of the chip groove, 10° rake angle and 15° clearance angle efficiently delivers the optimal performance. Besides, cutting performance of numerous coated tools was also studied. Results typically show that the multi-tooth milling tool with a diamond coating maintains significant advantages in aspects of the tool life and costs compared with the uncoated and diamond-like carbon coating (DLC) coated tools.

Key words

CFRP; Multi-tooth milling tool; Optimization; Interlaminar damage suppression

1. Introduction

Carbon Fiber Reinforced Polymers (CFRP) has excellent mechanical properties, such as an excellent specific strength and a great corrosion resistance; thus, it is widely used in

automobiles, aviation, and aerospace [1,2,3]. Although, CFRP are commonly manufactured by the near-net forming, most of the CFRP parts typically need to be properly trimmed in order to meet the size and assembly requirements. The milling process is one of the most commonly used methods for trimming of the CFRP [4,5]. However, due to the lower interlaminar bonding strength, the CFRP parts are prone to delamination damage during the CFRP machining, which has a substantial effect on the service performance of the CFRP parts [6]. Therefore, low-delamination milling of the CFRP remains a key factor which generally affects the further application of the CFRP.

Many valuable researches on optimizing the CFRP milling process have been carried out, primarily focusing on two key aspects: machining parameters and the milling tool. It was reported that the machining damage of the CFRP can hardly be completely suppressed by machining parameters optimization alone [7]. The milling tool in common is in direct contact with the CFRP in the milling process, its optimization can alter the cutting behavior, which provides a greater possibility for the damage suppression. Robert et al. [8] studied the surface quality in the milling of CFRP with different rake angles and clearance angles. It was reported that increasing the rake angle exerted a positive effect on the surface quality, and increasing the clearance angle progressively increased the milling quality due to the reduction of contact area between the tool and the material. Jenarthanan et al. [9] conducted a CFRP milling experiment with different helix angles. It was found that the helix angle was the most significant machining parameter affecting multiple performance characteristics. Han et al. [10] carried out experiments to compare the performance of the milling tool with diamond coated and TiB_2 coated. Results showed that the multi-tooth tool with diamond coated demonstrated the best performance with the smallest cutting force and the least wear.

However, during the milling process, conventional milling tools with helix flutes would typically produce an axial cutting force, which can cause delamination and burr of the upper surface due to the lower interlaminar bonding strength [11,12]. Therefore, further studies retain specific focus on the novel tool structure. Wang et al. [13] pointed out that the thrust force was the prime concentrated force causing the considerable damages in milling and proposed the left-right edge milling tool. For the upper surface, the left-right edge milling tool can cut forward inside, and minimize the cutting force (due to the left-handed spiral offset effect). Compared with the right edge milling tool, the left-right edge milling tool can effectively remove the burrs, and avoid delamination and the tears. Lopez et al. [14] designed a multi-tooth tool for CFRP milling. It was reported that the multi-tooth tool could not produce a Z-axis force component, and the bending of the slender workpieces by an effect of the cutting force was prevented. Wang et al. [7] optimized the structure of the multi-tooth cutter. In contrast with the conventional multi-tooth cutter, the multi-tooth cutter whose right-handed micro cutting edges and left-handed micro cutting edges were arranged alternatively in the cutter's circumferential direction had an obvious advantage in suppressing the surface damages in edge trimming of the CFRP. Overall, by optimizing the milling tool, the surface quality can be improved effectively. However, because it is challenging to properly obtain the interlaminar stress, scarce research optimized the geometry of the multi-tooth cutter directly exploiting the using interlaminar stress or damage.

In this work, a 3D finite element model for the milling of the CFRP is carefully developed. Additionally, cutting forces, interlaminar stress and interlaminar damage are properly presented. Moreover, the geometries of the multi-tooth milling tool are optimized by adopting a simulating model, and the tool coating is also optimized by the milling experiment.

2. 3D finite element model for milling of the CFRP

2.1 CFRP damage theory

Material property essentially remains an important factor to establish an accurate 3D finite element model. In our experiment, to give consideration to both computational efficiency and precision, we established a 3D finite element macro model. The single-layer plates were set as the equivalent homogeneous (EHM) model without distinguishing between fiber and matrix [15,16].

For the internal damage of the layer, the damage evolution model was established based on the CFRP 3D Hashin failure criterion [17,18,19]. Moreover, for the interlaminar damage, based on the Quade Damage, the layers were connected by the Cohesive elements to simulate the generation and expansion of interlaminar damage.

2.2 3D finite element model setting

The workpiece included laminated plates and interlaminar parts, as shown in the Fig. 1. In consideration of calculation efficiency, the model size of the workpiece was 5mm×3mm×2mm, and it was divided into four layers, each layer was 0.5mm in thickness. Cohesive elements were arranged between layers. The workpiece of the FE model was divided in to 4 layers, there were exactly 3 layers Cohesive elements, and the 3 layers Cohesive elements were the upper layer, middle layer and lower layer respectively, which can obtain the interlaminar damage of the upper layer, middle layer and lower layer when milling CFRP. The 1mm wide workpiece area on the side away from the cutting area was set to be fully constrained. In order to save the calculation time, the milling tool was defined as a rigid body because the rigidity of the milling tool was considerably greater than that of the workpiece.

The setup of mesh was very important in the simulation of high deformation. We set the element mesh type of laminated plate as C3D8R, and the generation mode was Structured Hex. The element mesh size of the laminated plate was 0.1mm×0.1mm×0.1mm, and the element number of the laminated plates were 34500. Further, the element mesh type of interlaminar the Cohesive element was positioned as COH3D8, and the generation mode was Sweep Hex. The thickness of the interlaminar Cohesive element was set as 0.01mm, and the mesh size was 0.1mm×0.1mm×0.01mm. Additionally, the element mesh type of the milling tool was set as C3D4, and the generation mode was Free Tet. The element mesh size of the milling tool was 0.3mm, and the element number of the milling tool was 76000.

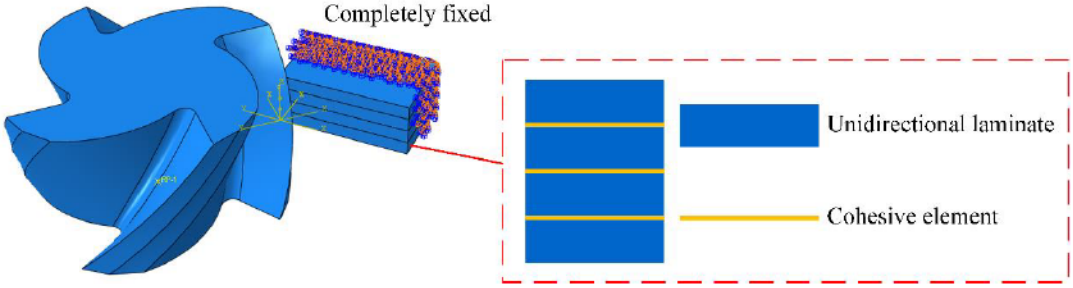

Fig. 1. Finite element model for milling CFRP

The motion of the reference point on the tool was controlled to realize the simulation of

the milling motion process. The contact between the milling tool and workpiece was stationed as the surface (milling tool) and the node region (all the nodes of the workpiece). The contact type was Coulomb friction, and the friction coefficient was 0.5 [20]. At the same time, in order to avoid the internal elements of the workpiece embedded in each other during the milling process, self-contact was adopted for the whole model. The parameters of the tool geometry and the milling process parameters are listed in Table 1 and Table 2, respectively.

Table 1 Geometrical parameters for the milling tool

Parameter	Value
Diameter, ϕ (mm)	10
Rake angle of the peripheral edge, γ (°)	10
Clearance angle of the peripheral edge, α (°)	10
Helix angle, λ (°)	45

Table 2 Milling process parameters

Spindle rotation Speed, n (rpm)	Feed speed, f (mm•r^{-1})	Axial depth, a_p (mm)	Radial depth, a_e (mm)
4000	0.24	2	1

2.3 Validation of the finite element model

In order to verify the accuracy of the finite element model, milling experiments were carried out. Fig. 2 shows the experimental setup for the milling of the CFRP. Milling processes were conducted on the DMU 80T vertical machining center. The CFRP workpieces were fixed by the two plates, and then they were installed on a dynamometer. Cutting forces were measured by the three-component dynamometer (Kistler™ 9257B).

In this work, the CFRP workpiece was unidirectional laminated plate, and the workpiece size was 250mm×120mm×2.5mm. Moreover, the carbon fiber was T700. The main properties of the CFRP are listed in Table 3. Right-hand carbide milling tools with 4 cutting edges and 10 mm diameter were used for the experiment, and the structural parameters of the milling tool were the same as those in the simulation model (Listed in Table 1).

In the experiments, we conducted four typical fiber orientation angle up milling processes. The axial depth was 2.5mm, which was different from the axial depth in the simulation. Because the increase in the axial depth in the simulation would lead to a sharp increase in the calculation time; thus, the axial depth in the simulation was kept smaller than that in the experiments, and the cutting force per unit depth (N•mm^{-1}) was used for the verification in the comparison process to ensure the unity of the comparison. Other cutting parameters are listed in Table 2.

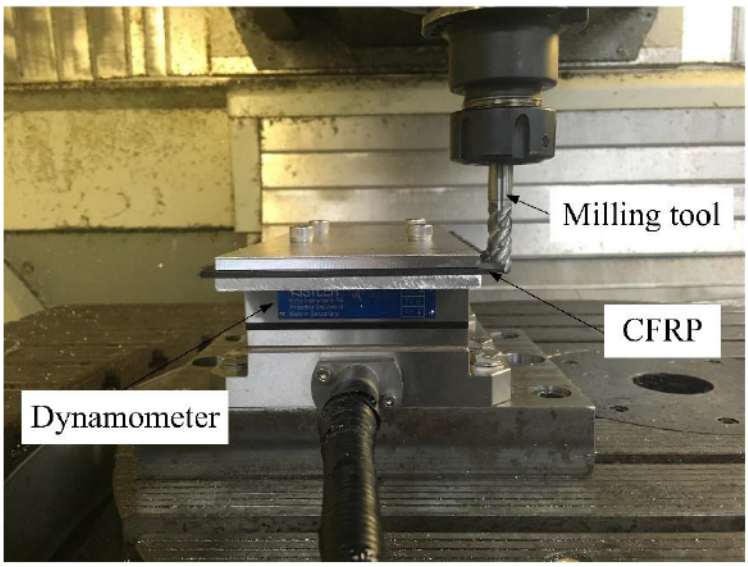

Fig. 2. Experimental setup for milling of the CFRP

Table 3 Material properties of CFRP

Property	Value
Elasticity modulus E_{11}/GPa	133
Elasticity modulus E_{22}/GPa	8
Elasticity modulus E_{33}/GPa	8
Shear modulus of the plane 1-2 G_{12}/GPa	5.32
Shear modulus of the plane 1-3 G_{13}/GPa	5.32
Shear modulus of the plane 2-3 G_{23}/GPa	3.99
Poisson's ratio v_{12}	0.25
Poisson's ratio v_{13}	0.25
Poisson's ratio v_{23}	0.34
Tensile strength along the fiber σ_{11}^{T}/MPa	1900
Compressive strength along the fiber σ_{11}^{C}/MPa	1300
Tensile strength perpendicular to the fiber σ_{22}^{T}/MPa	41
Compressive strength perpendicular to the fiber σ_{22}^{C}/MPa	170
Shear strength in the plane 1-2 S_{12}/MPa	81
Shear strength in the plane 1-3 S_{13}/MPa	81
Shear strength in the plane 2-3 S_{23}/MPa	81
Tensile fracture energy along the fiber direction G_{ft}/(N·mm^{-1})	81.5
Compression fracture energy along the fiber direction G_{fc}/(N·mm^{-1})	106.3
Tensile fracture energy perpendicular to the fiber direction G_{mt}/(N·mm^{-1})	0.28
Compression fracture energy perpendicular to the fiber direction G_{mc}/(N·mm^{-1})	1.31
Mass density ρ/(Kg•m^{-3})	1210

The average values of the peak cutting force in the stable cutting zone were typically

taken as the experimental and simulated cutting forces. Fig. 3 shows the cutting forces of the milling CFRP unidirectional laminated plates. The cutting forces obtained by the simulation were mostly smaller than those by the experiment, which is ascribed to the ideal condition that the tool of the simulation model was completely sharp and without wear. The average errors between the experimental results and the simulation results of four typical fiber orientation angles in X (F_x), Y (F_y) and Z (F_z) directions were 28.5%, 16.9% and 13.4% respectively. By comprehensive and careful considerations of the variations and values of the cutting forces, the 3D finite element model was reliable to be used for the geometric optimization of the cutting tool in the milling of CFRP.

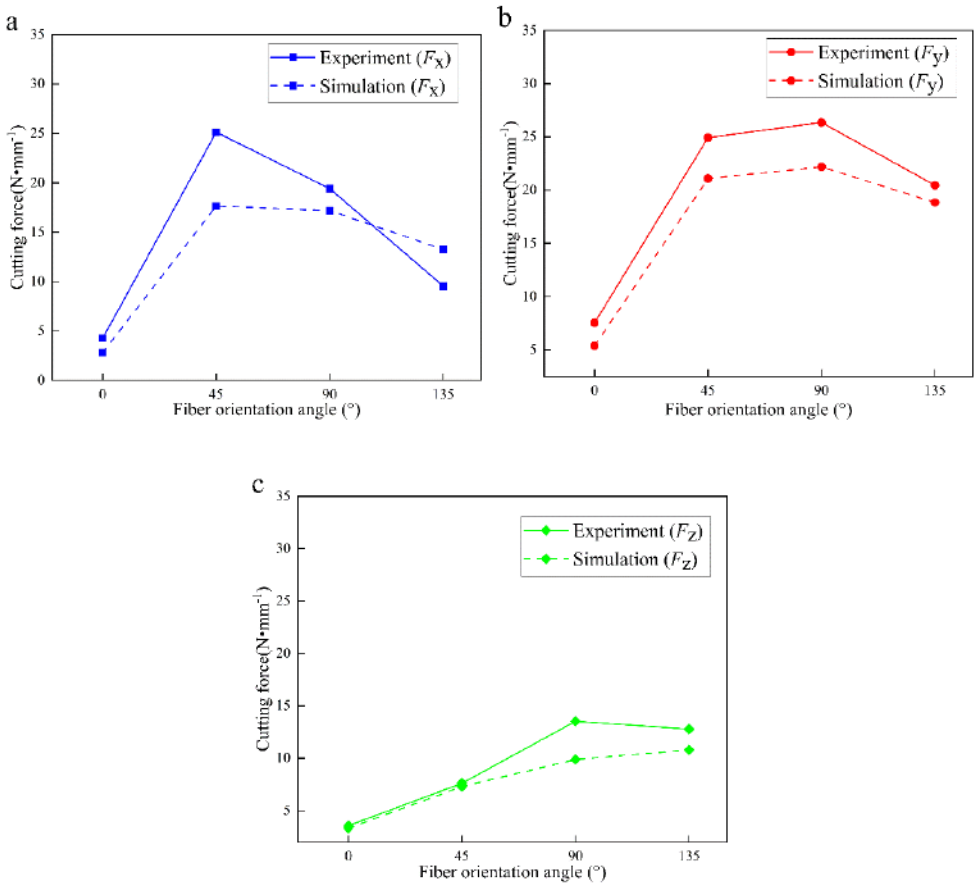

Fig. 3. Cutting forces in different fiber orientation angles (a) F_x (b) F_y (c) F_z

2.4 Characterization of the interlaminar damage

Milling of the CFRP is susceptible to interlaminar crack, tear, and delamination due to the lower interlaminar bonding strength. So, decreasing the interlaminar stress is always a goal in the machining of CFRP. However, it is difficult to measure the interlaminar stress by experiments. In our experiment, the interlaminar stress was extracted based on the 3D finite element model. 16 nodes of 4 elements at a certain distance from the cutting area (ensure 16 nodes were not removed during the entire cutting process) were used as stress extraction nodes, and the interlaminar stress was expressed with the Mises equivalent stress [21], as shown in the Fig. 4. As it is known that greater the average value of the interlaminar stress at the same location, the more serious is the interlaminar damage; thus, we took an average stress of 16 nodes as a reference standard of the interlaminar stress.

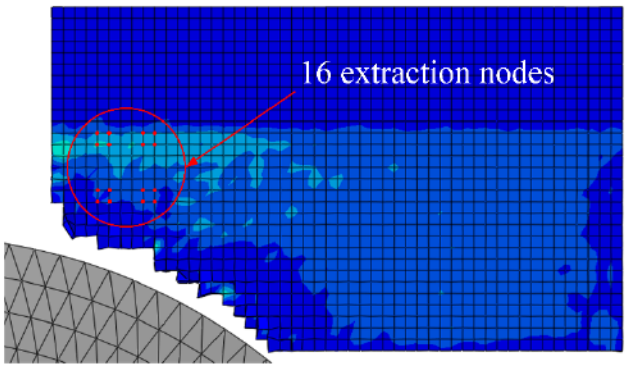

Fig. 4. Extraction node of interlaminar stress

The quantitative characterization of the interlaminar damage is very important for the comparison of the interlaminar damage under the different processing conditions. During the cutting process, the stiffness degradation occurs when the stress of the interlaminar element reaches the extreme value under the action of the cutting force. It was reported that when the stiffness degradation reaches 0.99, the material has almost lost its bearing capacity and can be used as the interlaminar damage area [22]. Therefore, in this experiment, the area where the stiffness degradation coefficient reached to 0.99 was regarded as the interlaminar damage area. In this work, the 2D interlaminar damage factor was used to calculate and characterize the interlaminar damage [23], as shown in the Fig. 5. The 2D interlaminar damage factor F_{d} is given as

$$F_{\mathrm{D}} = \frac{A_{\mathrm{D}}}{A_{\mathrm{T}}} \tag{1}$$

where A_{D} is the area of the interlaminar damage area and A_{T} is the area of the material to be removed. A_{T} can be calculated by

$$A_{\mathrm{T}} = a_{\mathrm{e}} \times L \tag{2}$$

where a_{e} is the radial depth of milling and L is the length of the workpiece to be machined.

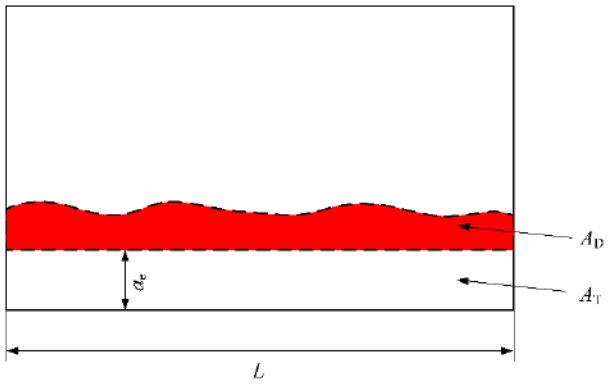

Fig. 5. Schematic diagram of 2D interlaminar damage factor characterization

It was reported that when the milling tool was right-hand milling tool, the cutting edge produced an upward cutting force component, due to the constraint of the upper layer of the CFRP was weak, the interlaminar damage of the upper layer was more serious than that of the lower layer [11,13]. In our experiment, the interlaminar stress of the upper interlaminar Cohesive elements of the CFRP was used to characterize the milling damage of the CFRP.

3. Optimization of the milling tool

3.1 Optimization of the geometrical parameters

The geometric parameters of the multi-tooth milling tool, including the helix angle, the section shape of the chip groove, the rake angle and the clearance angle, would be optimized by the established milling simulation model.

3.1.1 Helix angles of the grooves and numbers of the grooves

Left-handed chip grooves and the right-handed helix grooves interleaved to form the micro tooth (Fig. 6), so the structure of the micro tooth depends on the left and right helix angles and the number of the left-handed and right-handed grooves.

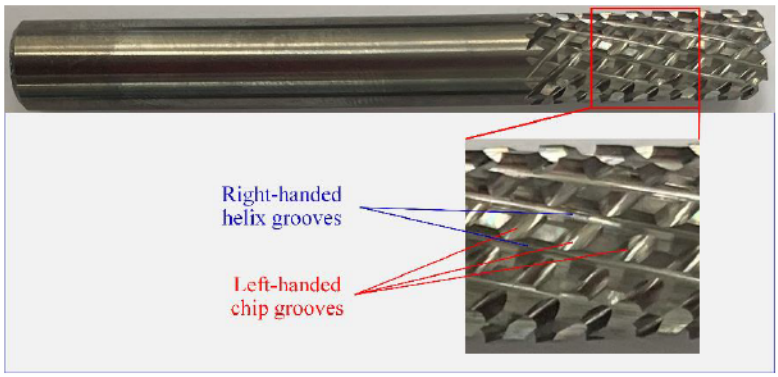

Fig. 6. The structure of the multi-tooth milling tool

As shown in the Fig. 7, the left helix angle and the number of the left-handed chip groove can be calculated as

$$l_{AC} = \frac{\pi \times d}{m} \tag{3}$$

$$l_{BC} = l_{CD} \times \sin\beta \tag{4}$$

$$l_{BD} = l_{CD} \times \cos\beta \tag{5}$$

$$\alpha = \operatorname{acrtan} \frac{l_{AB}}{l_{BD}} \tag{6}$$

$$l_{EF} = l_{CE} + l_{FD} \tag{7}$$

where d is the diameter of the multi-tooth milling tool, in this work, the diameter of the multi-tooth milling tool is 10mm, m is the number of the left-handed chip groove, α is the left helix angle, β is the right helix angle, and the length of the micro-edge is l_{EF}.

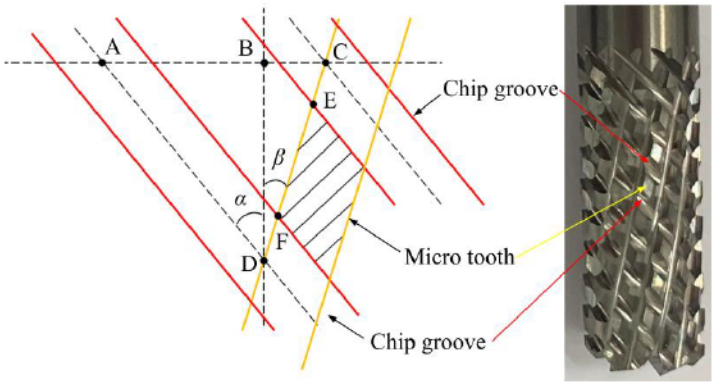

Fig. 7. The calculation of the left-handed helix angle

More teeth can effectively improve the tool life and machining efficiency. Due to the small CFRP chips, the number of right-handed helix groove for 10mm diameter tool is usually 8-14. In our experiment, the number of right-handed helix groove was set at 12 and the length of micro edge was set at 1.4mm. The number of teeth and micro edge length are not discussed in this paper.

Table 4 shows the different parameters of the left helix angle and the number of left-handed chip groove, the multi-tooth milling tools with different left helix angle and number of the left-handed chip groove are shown in the Fig. 8.

Table 4 Multi-tooth milling tool with different left helix angle and the number of left-handed chip groove

Serial number	Left helix angle α (°)	Number of the left-handed chip groove, m	Right helix angle β (°)
1	64.1	5	15
2	45.6	9	15
3	41.8	10	15
4	38.2	11	15
5	26.9	15	15
6	63.5	5	25
7	42.3	9	25
8	37.7	10	25
9	33.4	11	25
10	19.7	15	25

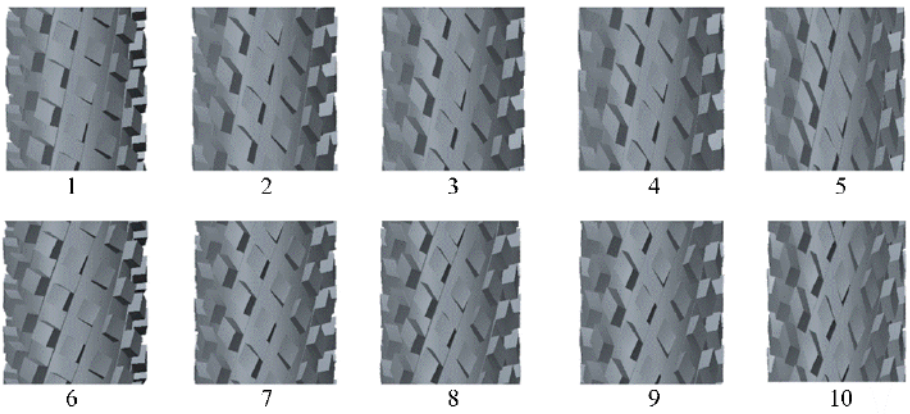

Fig. 8. Multi-tooth milling tools with different left helix angle and number of the left-handed chip groove

Fig. 9 shows the cutting forces with the different left helix angles and number of the left-handed chip grooves. Because the Y direction was the feed direction, so the cutting force in the Y direction was greater than that in the other two directions. Whether the right helix angle is 15° or 25°, the axial force decreases first and then increases with the increase of the number of the left-handed grooves. When the number of the left-handed groove was 11, the axial force was the minimum, and the left helix angle was 38.2° and 33.4°, respectively. Fig. 10 shows the interlaminar stress and 2D interlaminar damage factor with the different left helix angles and number of the left-handed chip grooves. The variation trend of the interlaminar stress and 2D interlaminar damage factor was basically consistent with that of the axial force. When the axial force was minimum, the interlaminar stress was minimal, correspondingly, the interlaminar damage was insignificant.

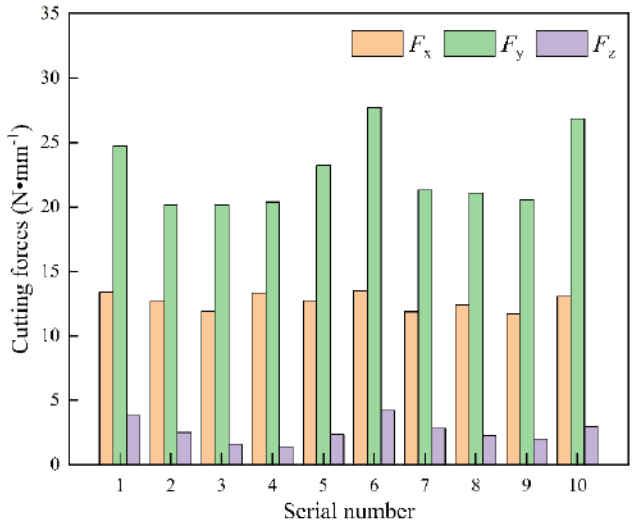

Fig. 9. Cutting forces with different left helix angles and number of the left-handed chip grooves (fiber orientation angle= 45°, n= 4000rpm, f= 0.24 mm•r^{-1}, a_p= 2mm, a_e= 1mm)

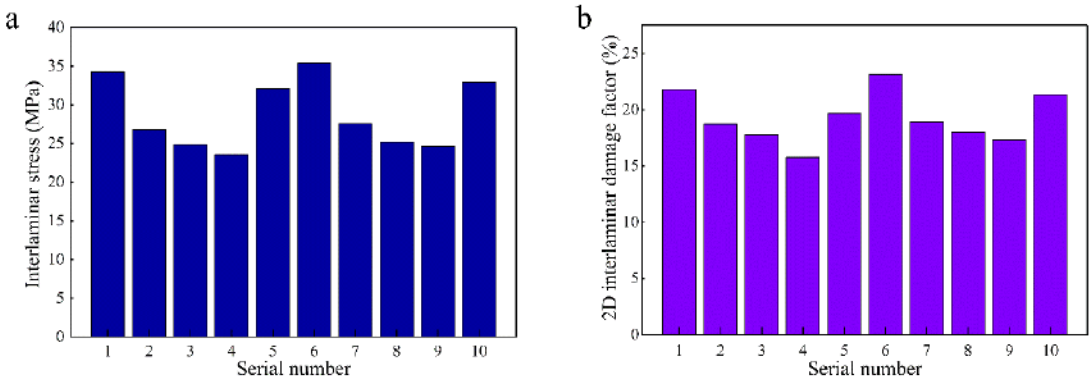

Fig. 10. Interlaminar stress and 2D interlaminar damage factor with different left helix angles and number of the left-handed chip grooves (a) interlaminar stress (b) 2D interlaminar damage factor (fiber orientation angle= 45°, n= 4000rpm, f= 0.24 mm•r^{-1}, a_p= 2mm, a_e= 1mm)

The axial force should be determined by both the left helix angle and the length of the micro tooth in the direction of the chip groove. As shown in the Fig. 8 and Fig. 11, with the increase of the number of the left-handed chip groove, the left helix angle decreases, in addition to decrease in the downward axial force generated by the left-handed chip groove. Further, the effect of the reduced downward axial force offsetting the upward axial force generated by the right-handed helix groove is reduced, so the overall axial force increases with the increase in the number of the left-handed chip groove. However, with the increase in the number of the left-handed chip groove, the micro tooth become longer in the direction of the chip groove, as shown in the Fig. 8. As the micro tooth become longer, the cutting length of the micro tooth which produces downward axial force is increased, making downward axial force generated by the left-handed chip groove to increase, so the overall axial force is decreased with the increase in the number of the left-handed chip groove. Therefore, the number of left-handed chip groove should consider both the left helix angle and the effective cutting length of the micro tooth. Compared with the right helix angle of 25°, the axial force with the right helix angle of 15° is smaller. As shown in the Fig. 8 and Fig. 11, with the decrease in the right helix angle, the upward axial force generated by the left-handed chip groove is decreased, so the overall axial force decreases with the decrease in the right helix angle.

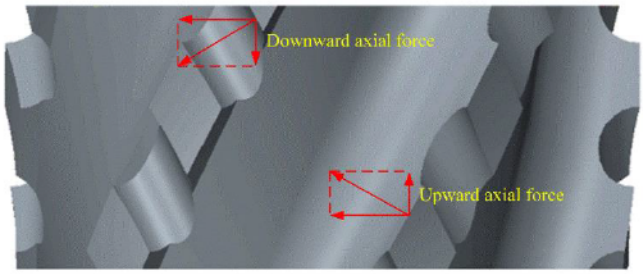

Fig. 11. Diagram of force applied by milling tool

3.1.2 Section shape of the chip groove

The section shape of the chip groove is an important parameter that can affect the cutting behavior of the chip groove. The most commonly used section shapes of the chip groove includes: approximate rectangular and the arc, as shown in the Fig. 12.

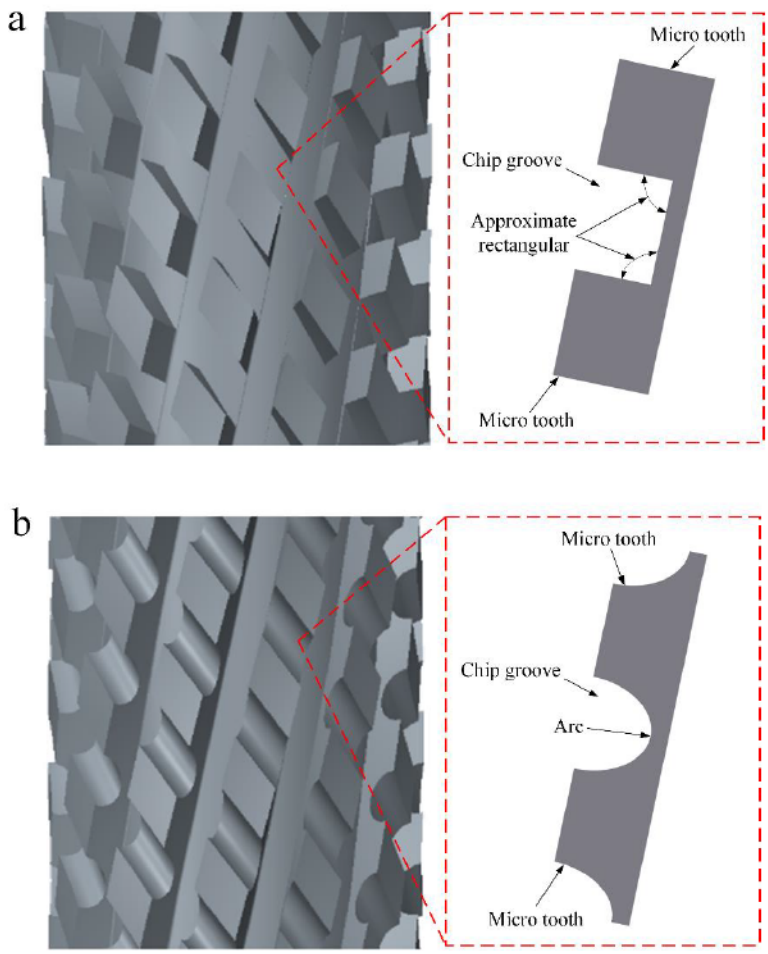

Fig. 12. Multi-tooth milling tools with different section shape of the chip groove

(a) Approximate rectangular (b) Arc

Fig. 13 shows the cutting forces with different section shape of the chip grooves. Compared with the axial force of an arc section shape chip groove, the axial force of approximate rectangular section shape chip groove is reduced by 46.9%. Because the Y direction was the feed direction, so the cutting force in the Y direction was greater than that in the other two directions. Fig. 14 shows the interlaminar stress and 2D interlaminar damage factor with different section shape of the chip grooves. Compared with the 2D interlaminar damage factor of an arc section shape chip groove, the 2D interlaminar damage factor of approximate rectangular section shape chip groove is reduced by 17.8%. As mentioned above, the smaller axial force corresponds to the smaller interlaminar stress and interlaminar damage.

As shown in the Fig. 12, an arc shape groove produces a negative rake angle for the left-handed cutting edge, which can produce large axial forces. It was reported that the approximate rectangular shape left-handed cutting edge was sharper than an arc shape

left-handed cutting edge, which could produce smaller cutting forces [24]. So, the overall axial force of an arc shape should be smaller, and the interlaminar damage of an arc shape will be smaller. However, this is inconsistent with the results. Considering that the rake face of the arc shape groove is an arc, this may be related to the axial force direction generated by the left-handed cutting edge. The direction of the axial force generated by the approximate rectangular shape left-handed cutting edge is unchanged, while the direction of the axial force generated by the arc shape left-handed cutting edge is changed. Therefore, the approximate rectangular shape left-handed cutting edge can effectively offset the axial force generated by the right-handed cutting edge, which can produce smaller overall axial force, resulting in less interlaminar damage.

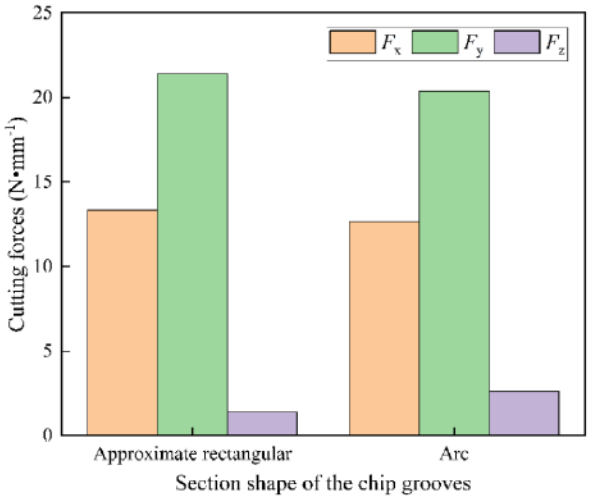

Fig. 13. Cutting forces with different section shape of the chip grooves (fiber orientation angle= 45°, n= 4000rpm, f= 0.24 mm•r^{-1}, a_p= 2mm, a_e= 1mm)

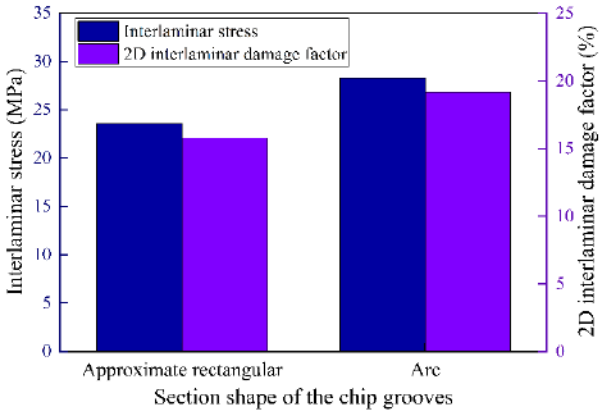

Fig. 14. Interlaminar stress and 2D interlaminar damage factor with different section shape of the chip grooves (fiber orientation angle=45°, n=4000rpm, f=0.24 mm•r^{-1}, a_p=2mm, a_e=1mm)

3.1.3 Rake angle and clearance angle

The rake angle and clearance angle are important parameters that can affect the cutting behavior of the micro tooth. Fig. 15 shows the cutting forces with different rake angles and clearance angles. Because the Y direction was the feed direction, so the cutting force in the Y direction was greater than that in the other two directions. As shown in the Fig. 15a, with the increase of the rake angle, the axial force decreases, because the larger rake angle can make the micro tooth become sharper. Whether the rake angle is 10° or 20°, there is no significant

difference in the magnitude of the axial force. Considering that excessive rake angle reduces the strength of the tool tip, and the high strength of the carbon fiber can cause tool wear, so the rake angel of 10° is selected. As shown in the Fig. 15b, with the increase of the clearance angle, the axial force decreases, because the large clearance angle can reduce the friction between the flank surface of the micro tooth and the workpiece, and make the micro tooth become sharper. Whether the clearance angle is 10° or 15°, there is no significant difference in the magnitude of the axial force. Because the large clearance angle can improve the wear resistance of the micro tooth, so the clearance angel of 15° is selected. Fig. 16 shows the interlaminar stress and 2D interlaminar damage factor with different rake angles and clearance angles. The smaller axial force corresponds to the smaller interlaminar stress, correspondingly, the interlaminar damage is smaller.

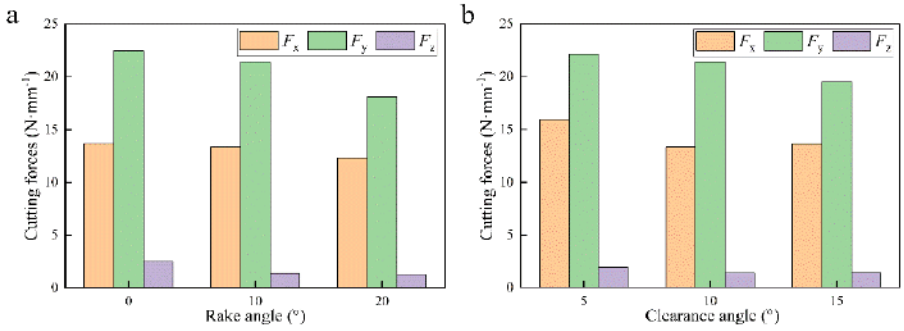

Fig. 15. Cutting forces with different rake angles and clearance angles (a) rake angle (b) clearance angle (fiber orientation angle= 45°, n= 4000rpm, f= 0.24 mm•r^{-1}, a_p= 2mm, a_e= 1mm)

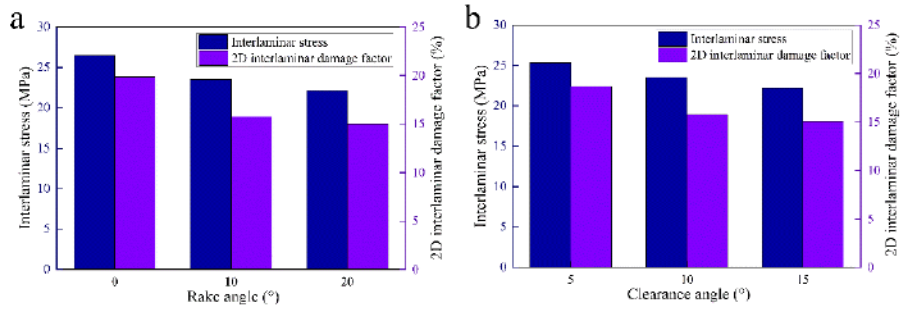

Fig. 16. Interlaminar stress and 2D interlaminar damage factor with different rake angles and clearance angles (a) rake angle (b) clearance angle

(fiber orientation angle= 45°, n= 4000rpm, f= 0.24 mm•r^{-1}, a_p= 2mm, a_e= 1mm)

Based on the 3D finite element model for the milling of CFRP and simulation results, the geometrical parameters of the multi-tooth milling tool are optimized and designed. The optimization results are listed in the Table 5.

Table 5 The optimized geometric parameters

Length of micro tooth	Left helix angle	Number of left-handed chip groove	Right helix angle	Number of right-handed helix groove	Section shape of the chip groove	Rake angle	Clearance angle
1.4mm	38.2°	11	15°	12	Approximate rectangular	10°	15°

3.2 Optimization of the tool coating

Diamond coating is commonly suggested for machining of the CFRP. Comparing to the diamond coating, diamond-like carbon coating (DLC) has relatively poor performance but lower cost, so DLC is also widely used for the cutting tool. In this experiment, the performances of the different tools were compared by milling experiments. Four types of milling tools i.e., conventional milling tool, multi-tooth milling tool, DLC coated multi-tooth milling tool, and diamond coated multi-tooth milling tool (as shown in the Fig. 17) were used to optimize the tool coating and to verify the cutting performance of the milling tool optimized by simulation. Due to the low Co content requirement of diamond coating, WC/6Co carbide was used for the substrate of diamond coated multi-tooth milling tool. The substrates of DLC coated multi-tooth milling tool and uncoated milling tools were the same, WC/12Co carbide. Multi-directional CFRP panel with $[45/0/-45/90]_{6s}$ orientation was used for the workpiece, and its size was 170mm×120mm×6mm. The helix angle of the conventional milling tool was 25°. The machining quality of the CFRP was measured by the Keyence™ VHX-1500 microscopy and the QUANTA FEG250 SEM. The tool wear was measured by the Microcapture pro microscope. The milling process parameters are listed in the Table 6.

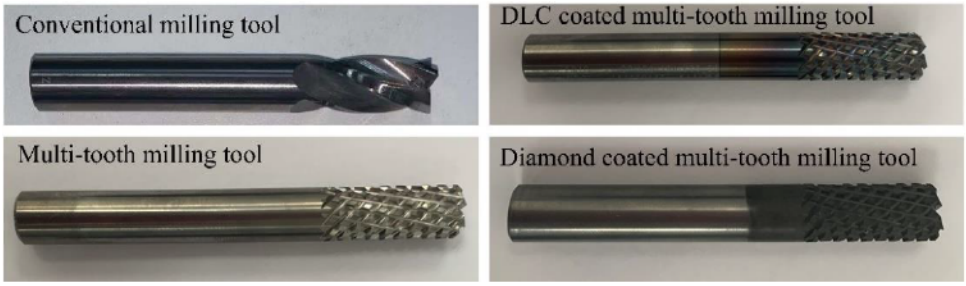

Fig. 17. The experimental tools

Table 6 Milling process parameters

Tool type	Spindle rotation Speed, n (rpm)	Feed speed, f_{zt} (mm•z^{-1})	Axial depth, a_p (mm)	Radial depth, a_e (mm)
Conventional milling tool	4000	0.06	6	1
Multi-tooth milling tool	5000	0.02	6	1

Fig. 18 shows the burrs at the upper surface and lower surface of the CFRP workpiece with different tools when the milling length was 1.7m. It can be found that the burrs of the CFRP workpiece machined with conventional milling tool is the worst. As mentioned above, the left-handed chip groove of the multi-tooth milling tool can generate the downward axial force, so the staggered left-handed chip grooves and right-handed helix grooves can generate cutting force reciprocating up and down on the fiber, and this effect is conducive to the fiber fracture. However, the conventional milling tool only has the right-handed helix grooves which only generate the upward axial force, and the fibers are not easy to break, so the burrs of the CFRP workpiece machined with the conventional milling tool is worse. Compared with the multi-tooth milling tool, the CFRP workpiece machined with coated multi-tooth

milling tool had almost no burrs. At the beginning of the milling process, the coated of the multi-tooth milling tool was not yet destroyed. The coated multi-tooth milling tool was sharper than the multi-tooth milling tool, so the coated multi-tooth milling tool could effectively remove fibers and avoid burring.

Fig. 19 shows the machined surface of the CFRP workpiece with different tools when the milling length was 1.7m. The result shows that there was no obvious difference between the different tools. It was stated that an increase in tool wear would lead to the increase of the axial force [25]. Although the uncoated tool wear is more serious, the uncoated tool wear may not cause a large increase in the axial force in the initial stage of the milling; therefore, no delamination damage is found on the CFRP workpiece machined by coated or uncoated tool.

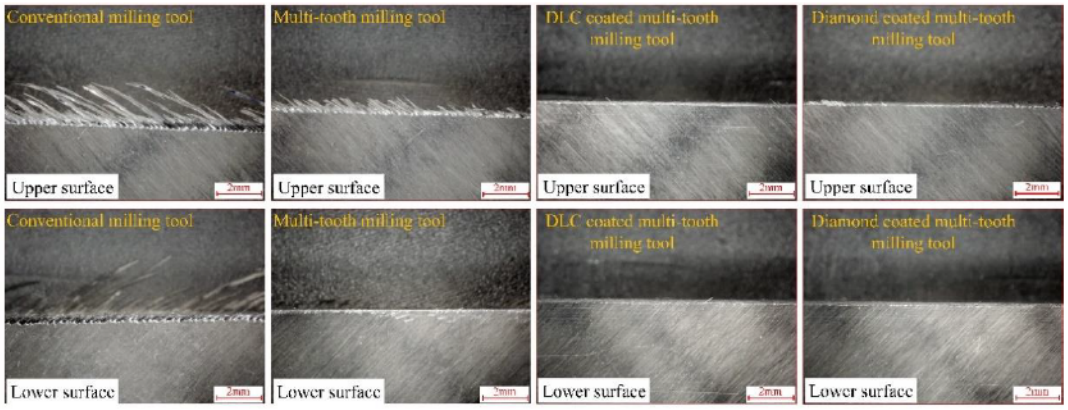

Fig. 18. The burrs at upper surface and lower surface of the CFRP workpiece with different tools (milling length: 1.7 m)

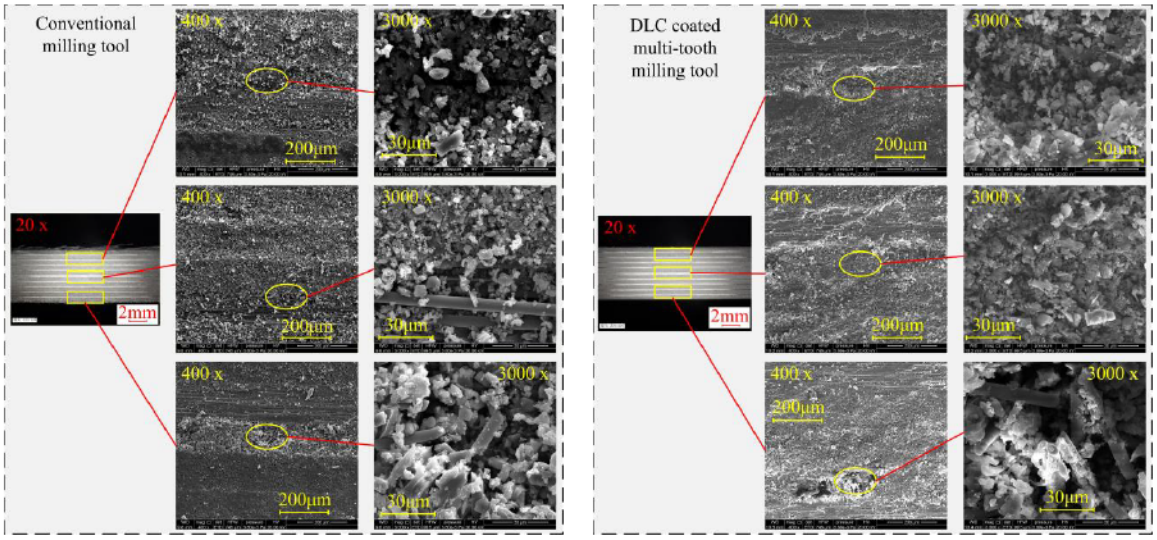

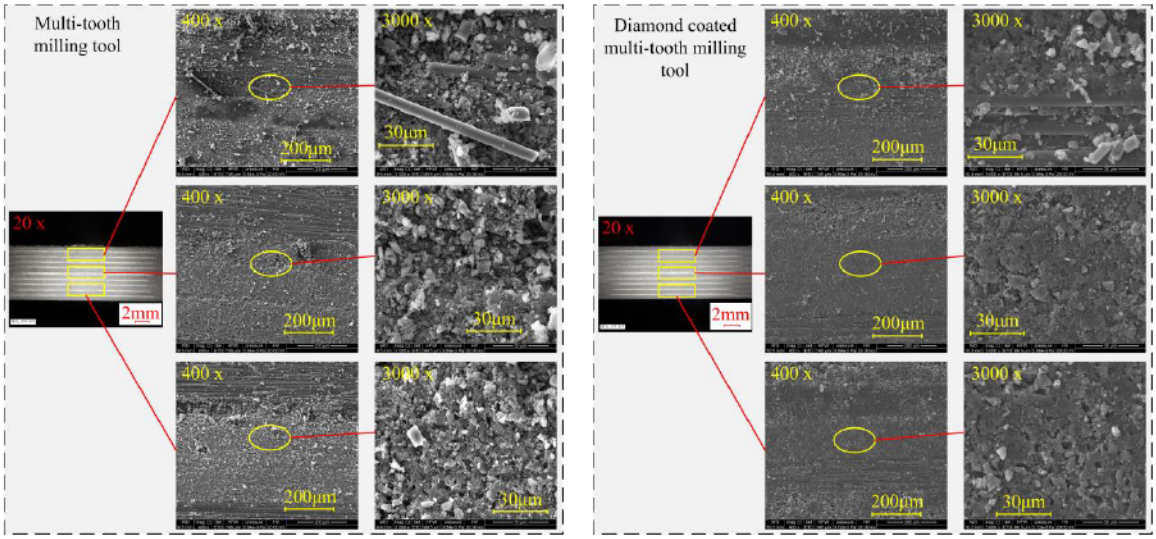

Fig. 19. The machined surface of the CFRP workpiece with different tools (milling length: 1.7m)

Fig. 20 shows the burrs at the upper surface and lower surface of the CFRP workpiece with different tools when the wear of the flank (VB) reaches 0.1mm. The CFRP workpiece machined with four types of the milling tools produces obvious burrs because of the tool wear. However, the burrs of the CFRP workpiece machined by the conventional milling tool was worse, the reason for this phenomenon has been explained above.

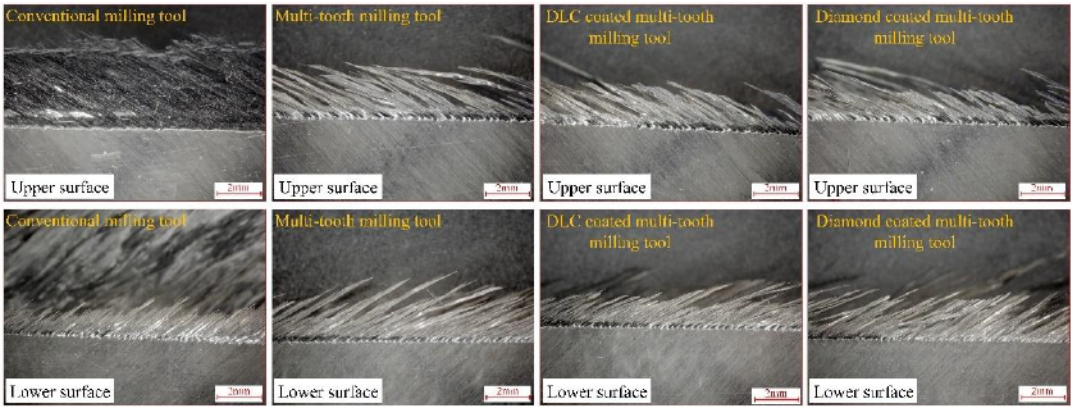

Fig. 20. The burrs at upper surface and lower surface of the CFRP workpiece with different tools (VB: 0.1 mm)

Fig. 21 shows the machined surface of the CFRP workpiece with different tools when the wear of the flank (VB) reaches 0.1 mm. Delamination occurred on the machined surface machined with uncoated tools, and the delamination was located on the upper part of the machined surface. It was stated that the multi-tooth tool with the diamond coated showed the smallest cutting force and the least wear extented under the same cutting parameter [10]. The cutting forces of the uncoated tools are larger and the constraint of the upper layer is weak; therefore, the delamination occurs.

Fig. 22 shows the tool wear when the wear of the flank (VB) reaches 0.1mm. The value of the wearing capacity of the flank (VB) was measured after every 1.7m milling. It can be found that the uncoated tools were passivated, this phenomenon can prove that the cutting

forces of the uncoated tools are larger. When milling the CFRP, although the left-handed chip grooves and right-handed helix grooves participate in the milling at the same time, the right-handed helix grooves plays a major role in milling, and the wear is more serious than the left-handed chip grooves. Note that, both the DLC coated and diamond coated were worn; however, the wear of the DLC coated was more serious. In addition, the variation of wearing capacity with the milling length was recorded, as shown in the Fig. 23. When the wear of the flank (VB) reaches 0.1mm, the milling length of the conventional milling tool, multi-tooth milling tool, DLC coated multi-tooth milling tool and diamond coated multi-tooth milling tool were 6.8 m, 11.9 m, 22.1 m, and 54.4 m respectively. That is to say, diamond coated multi-tooth milling tool has the longest service life, which was 8 times, 4.6 times, and 2.5 times than that of the conventional milling tool, multi-tooth milling tool, and DLC coated multi-tooth milling tool respectively. Our study shows, based on the manufacturing cost of the small batch production, the price of the diamond coated multi-tooth milling tool was 8.4 times, 1.3 times and 1.2 times than that of the conventional tool, uncoated tool and DLC coated tool respectively. Therefore, comprehensively considering the cutting performance, tool life and tool cost, the diamond coated multi-tooth tool may be the first choice for CFRP milling.

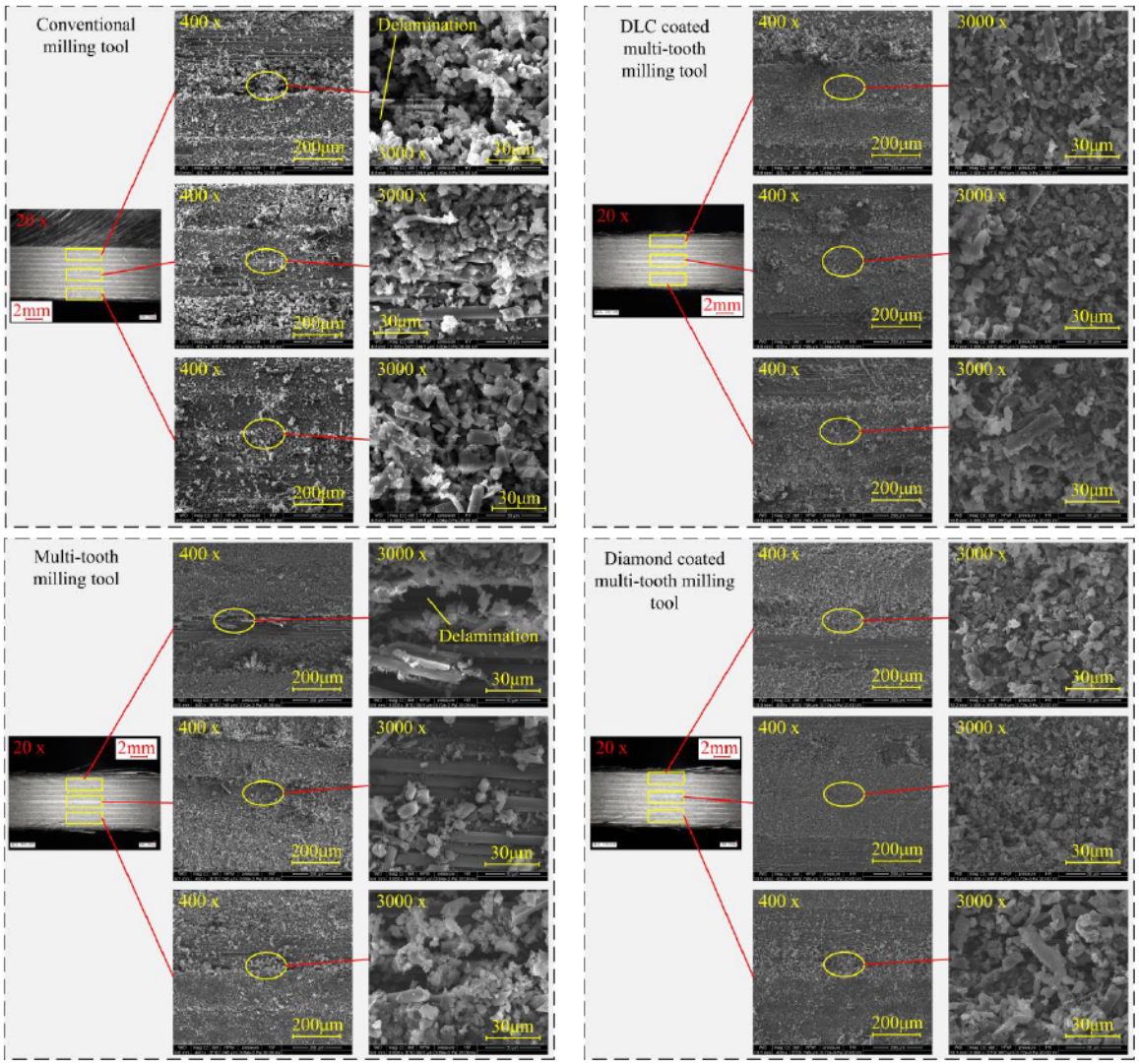

Fig. 21. The machined surface of the CFRP workpiece with different tools (VB: 0.1 mm)

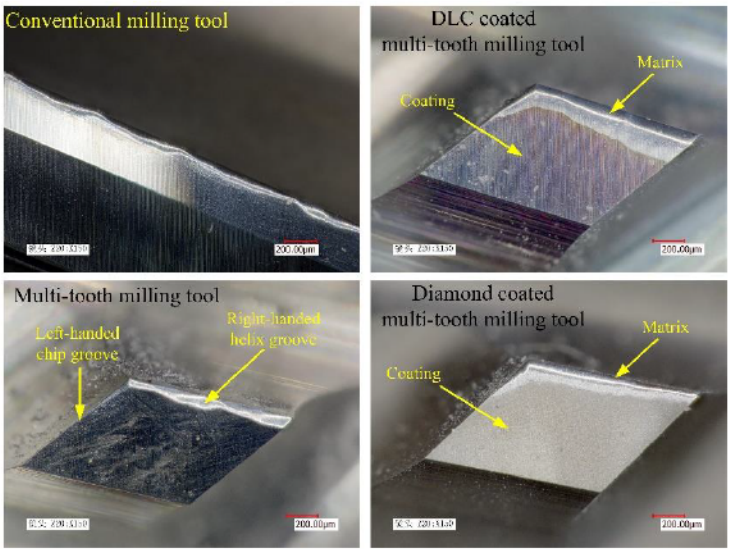

Fig. 22. Tool wear when the different tools meet the tool life standard

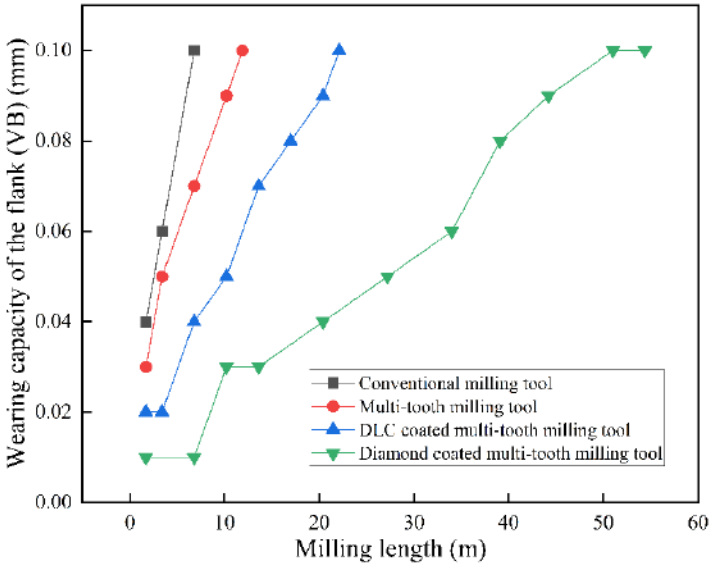

Fig. 23. The variation in wearing capacity of the flank with milling length

4. Conclusion

In this experiment, the 3D finite element model for the milling of CFRP was developed. Based on the 3D finite element model, the geometric parameters of the multi-tooth milling tool were optimized for the interlaminar damage suppression in the milling of CFRP. The performance of the optimized multi-tooth milling tool and the conventional milling tool was carried out by the experiments. The main conclusions are given as follows.

1. The left helix angle and the length of the micro tooth in the direction of the chip groove jointly affects the interlaminar damage. The downward axial force generated by the left-handed chip groove decreases with the decrease in the left helix. Additionally, when the effects of the reduced downward axial force offsetting the upward axial force is

reduced, the overall axial force increases. When the left helix angle decreases, the micro tooth become longer in the direction of the chip groove, the cutting length of the micro tooth which produces downward axial force increases, further increasing the downward axial force generated by the left-handed chip groove increase, as a result, the overall axial force decreased.

2. Compared with the arc section shape chip groove, rectangular section shape groove produced 17.8% less damage factor. It is related to the axial force direction generated by the left-handed cutting edge. The direction of the axial force generated by the approximate rectangular shape left-handed cutting edge is unchanged, while the direction of the axial force generated by the arc shape left-handed cutting edge is changed. The approximate rectangular shape left-handed cutting edge can effectively offset the axial force generated by the right-handed cutting edge, which can produce smaller overall axial force, resulting in less interlaminar damage.
3. There was no obvious difference in the interlaminar damage between the different rake angles and clearance angles. However, the wear resistance and sharpness of the micro tooth should be taken into consideration when selecting the rake angle and clearance angle of the micro tooth.
4. The right-handed helix grooves plays a major role in milling, and the wear is more serious than the left-handed chip grooves. Comprehensively considering the cutting performance, tool life and tool cost, the diamond coated tool is the first choice for CFRP milling comparing with the uncoated tool and DLC coated tool.

Acknowledgements

Funding The authors would like to acknowledge the financial support received from the Natural Science Foundation of China (No. 52075380 and 51775373) and the Natural Science Foundation of Tianjin (No. 19JCYBJC19000).

Author contribution Jian Liu: investigation, experimental design, data analysis, writing and editing. Xinkai Tang: finite element model, numerical and experimental data analysis, writing and editing. Shipeng Li: investigation, preparation of experimental materials, review and editing. Xuda Qin: investigation, preparation of experimental materials, review and editing. Hao Li: review and editing. Weizhou Wu: reivew and editing. Yadav Srijana: reivew and editing. Wentao Liu: reivew and editing. Haibao Liu: reivew and editing.

Data availability The data that support the findings of this study are available from the corresponding author upon reasonable request.

Code availability Not applicable.

Ethics approval Not applicable.

Consent to participate Not applicable.

Consent for publication Not applicable.

Competing interests The authors declare no competing interests.

References

1. Friedrich K, Almajid AA (2013) Manufacturing Aspects of Advanced Polymer Composites for Automotive Applications. Appl Compos Mater 20:107–128.
2. Geier N, Davim JP, Szalay T (2019) Advanced cutting tools and technologies for drilling carbon fibre reinforced polymer (CFRP) composites: A review. Compos Part A-Appl S 125, 105552. https://doi.org/10.1016/j.compositesa.2019.105552
3. Isbilir O, Ghassemieh E (2012) Finite Element Analysis of Drilling of Carbon Fibre Reinforced Composites. Appl Compos Mater 19:637–656.
4. Yashiro T, Ogawa T, Sasahara H (2013) Temperature measurement of cutting tool and machined surface layer in milling of CFRP. Int J Mach Tool Manu 70:63-69.
5. Wang FJ, Zhang BY, Ma JW, Bi GJ, Hu HB (2019) Computation of the Distribution of the Fiber-Matrix Interface Cracks in the Edge Trimming of CFRP. Appl Compos Mater 26:159–186.
6. Chen T, Gao F, Li SY, Liu XL (2018) The Comparative Study on Cutting Performance of Different-Structure Milling Cutters in Machining CFRP. Applied Sciences 8(8):1353.
7. Wang FJ, Zhang BY, Jia ZY, Zhao X, Wang Q (2019) Structural optimization method of multitooth cutter for surface damages suppression in edge trimming of Carbon Fiber Reinforced Plastics. J Manuf Process 46:204-213.
8. Voss R, Seeholzer L, Kuster F, Wegener K (2017) Influence of fibre orientation, tool geometry and process parameters on surface quality in milling of CFRP. CIRP J Manuf Sci Tec 18:75-91.
9. Jenarthanan MP, Jeyapaul R (2015) Analysis and optimisation of machinability behaviour of CFRP composites using fuzzy logic. Pigm Resin Technol 44(1):48-55.
10. Han SC, Chen Y, Xu JH, Zhou JW (2013) Experimental Study of Tool Wear in Milling Multidirectional CFRP Laminates. Materials Science Forum 770:276-280.
11. Liu HL, Zhang JB, Wang Z, Zhang JP, Li G (2013) Cutting tool selection in CFRP and AFRP machining. Aerospace Materials and Technology 43 (4):95-98.
12. Liu JD, Li YS, Yan GH, Huang LK, Yang XF, Yu DM (2015) Experimental Study on Surface Quality in Milling Carbon Fiber Reinforced Plastics. Key Engineering Materials 667:62–67.
13. Wang FJ, Yan JB, Zhao M, Wang D, Wang XN, Hao JX (2020) Surface damage reduction of dry milling carbon fiber reinforced plastic/polymer using left–right edge milling tool. J Reinf Plast Comp 39(11-12):409-42.
14. De Lacalle LNL, Lamikiz A, Campa FJ, Valdivielso AF, Etxeberria I (2009) Design and Test of a Multitooth Tool for CFRP Milling. J Compos Mater 43(26):3275-3290.
15. Mahdi M, Zhang L (2001) A finite element model for the orthogonal cutting of fiber-reinforced composite materials. J Mater Process Tech 113(1):373-377.
16. Arola D, Sultan MB, Ramulu M (2002) Finite Element Modeling of Edge Trimming Fiber Reinforced Plastics. J Manuf Sci E-T ASME 124(1):32-41.
17. Hashin Z (1980) Failure criteria for unidirectional fiber composites. J Appl Mech 47(2):329-334.
18. Hashin Z, Rotem A (1973) A fatigue criterion for fiber-reinforced materials. J Compos Mater 7(4):448-464.
19. Yang L, Yan Y, Kuang NH (2013) Experimental and numerical investigation of aramid fibre reinforced laminates subjected to low velocity impact. Polym Test 32(7):1163-1173.
20. Santiuste C, Soldani X, Maria HM (2010) Machining FEM model of long fiber composites for aeronautical components. Compos Struct 92(3):691-698.
21. Qin XD, Li YH, Wang B, Ji CH, Guo CY, Wang H, Xin HG (2016) Simulation of effect of fiber direction on cutting process of CFRP. Mech Sci Technol Aerosp Eng 35(3):472–476.
22. Phadnis VA, Makhdum F, Roy A, Silberschmidt VV (2013) Drilling in carbon/epoxy composites: Experimental investigations and finite element implementation. Compos Part A-Appl S 47:41-51.
23. Faraz A, Biermann D, Weinert K (2009) Cutting edge rounding: an innovative tool wear criterion in drilling CFRP composite laminates. Int J Mach Tools Manuf 49:1185-1196.
24. Niu B, Xu HZ, Zhang QC (2020) Effects of chip groove geometry parameters on milling composite using micro-tooth milling cutter. Tool Engineering 54(12):26-30.
25. Ishida T, Noma K, Kakinuma Y, Aoyama T, Hamada S, Ogawa H, Higaino T (2014) Helical milling of carbon fiber reinforced plastics using ultrasonic vibration and liquid nitrogen. Proc CIRP 24:13-8.

2022-05-27

Optimization of multi-tooth milling tool for interlaminar damage suppression in þÿ t h e m i l l i n g o f c a r b o n f i b e r r e i

Liu, Jian

Springer

Liu J, Tang X, Li S, et al., (2022) Optimization of multi-tooth milling tool for interlaminar damage þÿ s u p p r e s s i o n i n t h e m i l l i n g o f c a r b o n f i b e r r e i n f o r c e d p o l y m e r s , T h e I n t e r Advanced Manufacturing Technology, Volume 121, Issue 1-2, July 2022, pp.1235-1251

https://doi.org/10.1007/s00170-022-09369-9